archaeometry

Archaeometry ••, •• (2017) ••–•• doi: 10.1111/arcm.12306

'GUARD THE GOOD DEPOSIT':‡ TECHNOLOGY, PROVENANCE AND DATING OF BIPYRAMIDAL IRON SEMI-PRODUCTS OF THE DURRENENTZEN DEPOSIT (HAUT-RHIN, FRANCE)*

S. BAUVAIS,[1,2]† M. BERRANGER,[2] M. BOUKEZZOULA,[2] S. LEROY,[1,2] A. DISSER,[1,2] E. VEGA,[1,2] M. AUBERT,[2] P. DILLMANN[1,2] and P. FLUZIN[2]

[1]*LAPA-IRAMAT, NIMBE, CEA, CNRS, Université Paris-Saclay, CEA Saclay, Gif-sur-Yvette, France*
[2]*LMC, IRAMAT, UMR 5060, CNRS, Université de Technologie de Belfort-Montbéliard, Belfort, France*

In the early days of iron metallurgy in Western Europe, the most widespread type of 'trade iron' (semi-product) was bipyramidal in shape. Although they are frequently found, little is known about how they were manufactured and circulated, or even about their age. An interdisciplinary approach was applied to the Durrenentzen deposit (Haut-Rhin, France), the third-largest in Europe in terms of artefact quantities, in an attempt to reconstruct the technological, social and economic context that caused them to be abandoned. A morphometric study of the 51 iron bars revealed a high degree of homogeneity, despite variations in detail. Four objects were selected for archaeometric studies. Metallographic analyses show internal differences (quality of the material, nature of the alloys and manufacturing techniques). Chemical analyses also showed different provenances. Finally, radiocarbon analyses of the carbon in steel (iron/carbon alloy) linked this deposit to the early Iron Age. This study provided the first benchmark for more general research, significantly changing perceptions of the economics of iron at the beginning of the Iron Age.

KEYWORDS: TECHNOLOGICAL ANALYSIS, PROVENANCE STUDY, RADIOCARBON DATING, BIPYRAMIDAL BAR, IRON SEMI-PRODUCT, IRON TRADE, IRON AGE

INTRODUCTION

In Western Europe during the early period of iron metallurgy, one of the main types of 'trade iron' (semi-product) was bipyramidal in shape (Berranger and Fluzin 2012). A recent study (Berranger 2014) made a census of more than 1300 examples from more than 200 sites across Europe, from Great Britain to Poland. The main concentration essentially covers north-eastern France (for France, more than 450 objects from approximately 60 sites were inventoried) and western Germany (approximately 650 objects from 130 sites). Although they are frequently found, little is known about how they were manufactured and circulated, or even about their age. They were actually mainly discovered in isolated deposits, outside their functional context; that is, separate from any human occupation and with no other associated material. Whether the reason for their abandonment was economic (the hypothesis

*Received 30 August 2016; accepted 21 December 2016
†Corresponding author: email sylvain.bauvais@cea.fr
‡'Guard the good deposit' (2 Timothy 1:1–14)
© 2017 University of Oxford

of a blacksmith's cache) or ritual (known as votive), it led to the abandonment of considerable amounts of metal. By deducing an estimation from the mass of currently known objects of this form, nearly 6 metric tons of iron would have been abandoned in this way. Although the dating by their archaeological context is inaccurate, they have been variously attributed to the early Iron Age (Berranger 2014), the late Iron Age (Senn *et al.* 2014) or the Gallo-Roman period (Kleemann 1981). They are therefore essential sources of information to help understand the organization and circulation of the metal produced during these early periods.

Thanks to recent archaeometric methods to process analyses (Fluzin *et al.* 2011; Galili *et al.* 2015), provenance studies (Desaulty *et al.* 2009; Leroy *et al.* 2012; Disser *et al.* 2014, 2016) and dating of iron metals (Leroy *et al.* 2015a,b), we were able to envisage further clarification of as yet unanswered questions. These methods allow different levels of specialization among craftsmen to be determined; for example, by characterizing the know-how applied to the manufacture of intermediary products. As explained below, chemical analyses also make it possible to determine segmentation or continuity between different steps in the production process. This is particularly true for the steps between the smelting of iron ores and the manufacturing of semi-products (intended to be stored or exchanged). Finally, the main purpose of these methods is to determine whether the objects come from one or several production centres, to better understand how they were manufactured and traded.

The Durrenentzen deposit (Haut-Rhin, France) is the third-largest in Europe in terms of artefact quantities. It is located in the zone with the largest concentrations of this kind of bipyramidal bars (Fig. 1). The possibility of characterizing a series of trade iron of identical type and provenance motivated an interdisciplinary characterization study of this exceptional group of objects. There were several aims:

- To determine the nature of the materials and techniques used for their manufacture.
- To highlight, from a structural point of view, the specific features and common traits of objects from the same batch.

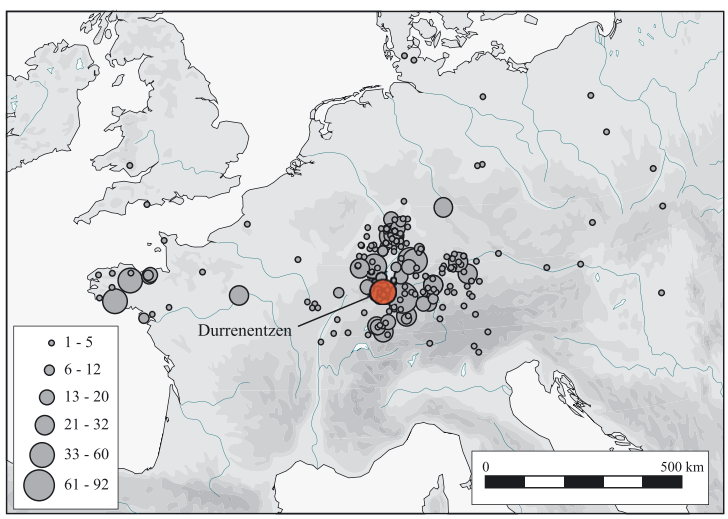

Figure 1 *A map showing the distribution of the bipyramidal iron bars and the location of the Durrenentzen deposit (red spot). [Colour figure can be viewed at wileyonlinelibrary.com]*

- To compare the origin of each metallic object by chemically characterizing the slag inclusions (SI) trapped within them.
- To date the objects by the radiocarbon method.

A GENERAL DESCRIPTION OF THE DISCOVERIES

Fifty-one bipyramidal bars were fortuitously discovered in the municipality of Durrenentzen in 1983, when a trench was dug for water pipes. An initial publication in 1986 (Biellmann 1986) described the context of the discovery and the macroscopic characteristics of the set of objects, along with the results of metallurgical analyses of two objects (DUR.3 and DUR.6). The conclusions indicated that the objects were poured into a mould and that impurities such as sulphur or phosphorus were extracted by refining. In the light of current knowledge about ancient metallurgy, these assertions are totally wrong.

The 51 bipyramidal bars are of a specific type, thinning towards the extremities by squeezing but without stretching. The sections are square or rectangular. They are attached to the BCS1 variant (short type of square section with squeezed extremities; Berranger 2014), which is currently one of the most frequently found. They must have undergone substantial refining work at least around their periphery, because they have no major pores or cracks on their surfaces. The extremities of several objects are missing.

The mass of the bars varies from 5500 to 6915 g, with an average of 6049 g (308.5 kg in total), and the length ranges from 215 to 331 mm (Fig. S1). The bars appear to be very homogeneous in terms of mass, length, width and thickness, with only minor morphological variations. Some of these reflect different finishing techniques, possibly linked to distinct individuals or workshops. An initial attempt to define a typology is proposed here, based on the forms of the central and lateral edges (Fig. S2). Four main types can be distinguished, although it is sometimes tricky to attribute a specific type to each of the bars in the deposit. Nevertheless, some main features can be distinguished without doubt; for example, between type 1, the general shape of which is best described as bipyramidal, and type 4, the morphology of which is closer to what is called 'fish-shaped' in other parts of the world (Pleiner and Bjorkman 1974). On the basis of this typology, four examples were selected for analyses. Two had already been cut up in the 1980s (DUR.3 and DUR.6).

METHODOLOGY AND EXPERIMENTAL FACILITIES

Metallographic observations

We first performed a metallographic analysis of the four bars (DUR.3, DUR.6, DUR.40 and DUR.48) in order to establish the quality of the materials, make a qualitative assessment of their chemical composition (iron/steel/phosphorus) and determine the manufacturing techniques used (demonstrable welding etc.).

The study protocol (Fluzin 2002) relies above all on morpho-metrological analyses that allow the sampling plane to be selected. After macrophotography, the objects were cut longitudinally along their widest side, to study the widest possible cross-section. The cutting was done using a water-jet to avoid any structural alterations due to heating. The sections obtained were polished with silicon carbide paper (grades 80 to 1200), then with diamond paste until 1 µm. They were observed as a whole under a metallographic microscope before and after chemical etching (nital 3% and Oberhoffer). Characteristic zones were recorded

by micrographic photography, and each section was illustrated either by a macrographic photograph or by an assembly of microphotographs (cartography).

Finally, image treatment software (LAS) was used to quantify the surface proportion of each constituent (inclusions and pores in particular). The relative error in the surface area calculation was estimated to be around 2%.

Chemical analyses of slag inclusions

The aim of the chemical analyses of slag inclusions (SI) applied in this paper was to understand how the deposit had been formed. It is possible to address this question by comparing the bars in terms of SI composition (Coustures *et al.* 2003; Desaulty *et al.* 2009; Leroy *et al.* 2012; Disser *et al.* 2014, 2016).

The chemical analysis protocol is in two steps.

The first step consists of characterizing the main component elements (i.e., > 0.5 wt% element) of inclusions in an object by energy-dispersive X-ray spectrometry (EDX with silicon drift detector) coupled with scanning electron microscopy (JEOL 7001-F model) of the transversal cross-section studied by metallography and previously carbon-coated. This method (scanning of the entire inclusion area) is described in detail in Disser *et al.* (2014). In particular, this step distinguishes smelting-related inclusions (carrying the chemical signature of the production area) from those generated during the post-reduction phases (forge) (Dillmann and l'Héritier 2007; Disser *et al.* 2014; Galili *et al.* 2015).

During the transformation of ores into metal, some oxides are not reduced: they become lithophilic and form slag, part of which remains trapped in the metal in the form of inclusions. These oxides—mainly MgO, Al_2O_3, SiO_2, K_2O and CaO—are called non-reduced compounds (NRC; Dillmann and l'Héritier 2007). Their relative compositions make up the signature of a smelting system, including the contributions of the ore, charcoal, furnace linings and possible fluxes (Dillmann and L'Héritier 2007). However, during the metal refining stage—where the aim is to transform the bloom into a bar—as well as during the more advanced smithing operations, it may be necessary to use additives for welding or to avoid oxidation of the metal. Some inclusions present in the metal can therefore arise partly or entirely from smithing additives and do not result at all, or only partly, from the smelting stage. Therefore, it needs to be checked that the inclusions considered are actually a result of smelting. The metallographic study thus first located possible welding lines within an object containing inclusions formed by additives. Next, the composition in major NRC elements allowed their characterization and differentiation from other non-polluted inclusions. It is also possible, when no welding line is visible by metallography, to characterize many inclusions chemically and, by statistical processing, to discriminate between the groups of inclusions whose signatures do not come from ores (Disser *et al.* 2014). These procedures were followed for each of the polished sections that were analysed, and allowed us to distinguish the groups of inclusions corresponding to the smelting stage. Only smelting-related inclusions will be discussed in this paper.

An average composition of the smelting SI, calculated for each metal mass by weighting the content of each SI by its area, was used to further compare the chemical composition of the SI (Dillmann and L'Héritier 2007), so that

$$\%E^* = \sum_{i=1}^{n} \left(\%E_i \times \frac{S_i}{S_T} \right),$$

where $\%E^*$ is the weighted content of the element or oxide considered; $\%E_i$ is the mass content of the element or the oxide in the i SI; S_i is the surface area of the i SI; S_T is the total surface area

of the analysed SI; and n is the total number of SI. In the following, these weighted contents will be indicated by an asterisk (%*).

Although MnO and P_2O_5 are not NRC (as they could be more dependent on local thermodynamic conditions), their mean values were considered. The FeO content is also entirely dependent on the local thermodynamic conditions. This is why, in order to discount the potential effects of enrichment, the average contents were normalized to 100% without the FeO content, in accordance with the formula proposed by Pagès *et al.* (2011). These surface-weighted contents normalized to 100% without FeO will henceforth be denoted with a double asterisk (%**).

The second step is the quantification of trace elements (i.e., < 0.1 wt% element) within selected reduction inclusions (approximately 10 per object), by using laser ablation – inductively coupled plasma – mass spectrometry (LA–ICP–MS). These analyses were carried out in the Ernest-Babelon Centre (IRAMAT, Orléans, France). The apparatus used was a VG Plasma Quad PQXS coupled with a Nd:YAG type laser with a quadrupled 266 nm wavelength. The laser beam diameter could be adjusted through a series of collimators and lenses from 40 to 200 µm. The size of the ablation is generally of the same order of magnitude as that of the inclusion, or sufficiently representative compared to the scale of the phases making up the inclusion. The analysis is therefore 'global' and the volume of the sample allows quantifications to be obtained that are representative of the entire inclusion. The detailed analytical methodology is described in Desaulty *et al.* (2009) and Leroy *et al.* (2012).

Thirty-nine chemical elements were measured, including the series of rare earth elements. Depending on the inclusion size and the Si content, and on the experimental conditions adopted, the limits of detection (LOD) reached varied from a few ppb to 15 ppm for all the elements except for Ti (LOD = 130 ppm). The relative error for these trace elements was between 5 and 10%.

To ensure pertinent statistical processing of the composition in trace elements (to address variations in scale in the composition), a specific logarithmic treatment of the data was chosen, following the method proposed by Leroy and Disser for inclusion studies (Leroy *et al.* 2012; Disser *et al.* 2014). For each element, an X_E value is calculated, which will be used afterwards:

$$X_E = \log([E]) - \frac{1}{N}\sum_{K=1}^{N}\log([E_K]),$$

where (E_K) are the N least variable and the best measured elements (never, or rarely, below the LOD). In our case study, the elements taken into account in the statistical analyses are Ce, Eu, Gd, La, Nd, Pr, Sm, Th, U and Y. The E_K elements are Ce, Eu, La, Sm and Y.

The multivariate and cluster analyses employed were: principal component analysis (PCA), based on a matrix composed of Pearson correlation coefficients; and agglomerative hierarchical clustering (AHC), by dissimilarity according to Euclidian distances and by Ward's aggregation method. The statistical treatments were carried out using the XLSTAT software, Version 2016.01.26779, from ADDINSOFT.

Radiocarbon dating

The four bipyramidal bars were dated by radiocarbon analysis. In the process of production of ancient iron and steelmaking, charcoal was used as a fuel to reduce into metal the oxides contained in the ore. During this transformation, part of the carbon can associate with iron in the form of cementite (iron carbide/Fe_3C), constituting the steely zones of the produced metal. Thus, extraction of the carbon from the metal and determination of its isotopic ratios allows carburized alloys to be dated.

The steely zones (which contain the carbon to be measured) are detected during the metallographic study of the object (see above). The preparation, collection and combustion of the samples collected followed a newly developed approach based on accelerator mass spectrometry (AMS), detailed in Leroy *et al.* (2015a,b). Finally, the CO_2 samples were reduced to graphite and measured by AMS in the LMC14 laboratory.

The radiocarbon dates obtained were transformed into calendar dates using the Oxcal 4.2.4 software (Ramsey and Lee 2013), which uses the IntCal 13 calibration curve (Reimer *et al.* 2013). Two radioactive measurements were obtained for each metallic mass, and dated to verify any potential 'old wood' effect. Because these two radiocarbon measurements were performed on the same metallic mass, they date the same event. We chose to combine them using the R-Combine tool in Oxcal to obtain an age density for each bar.

RESULTS

Metallographic characteristics

Inclusionary cleanliness The high variability among the samples is apparent. Impurities (pores and SI) occupy 3–17% of the surface areas observed, depending on samples (Table S1). Two bipyramidal bars are characterized by inclusionary cleanliness assessed as excellent (between 0 and 5%) according to established references for objects from the same period (Bauvais and Fluzin 2006). Of the others, one was assessed as 'good' in terms of inclusionary cleanliness (between 5 and 10%) and the last as 'poor' (between 15 and 25%).

The distribution of the impurities is equally variable. On DUR.40, they are most frequent on the periphery of the section studied, whereas on DUR.3 and DUR.6, they are mainly concentrated in the central part (Fig. 2). In this zone, their outlines are usually shredded, because they have only been slightly deformed by hammering.

Pores are more numerous in DUR.6, DUR.3 and DUR.48, due to incomplete consolidation, during which the pores that formed were not sufficiently crushed. Furthermore, in the example of DUR.48, the metal is locally mixed with a high proportion of small SI, showing incomplete agglomeration of the metallic matrix.

The inclusions within all the objects are multiphase and made up of fayalite-type iron silicates (Fe_2SiO_4), glassy phases and wüstite dendrites (FeO), in variable proportions (Fig. S3). Some are completely amorphous and siliceous. Moreover, DUR.40 and DUR.3 contain inclusions made up almost exclusively of wüstite globules embedded in a silicate matrix. Their formation is due to the insertion of iron oxides produced by metal hot-oxidation (hammer-scale) during the smithing operations. None of the surfaces of the bars showed any hammer-scale or peripheral slag toppings produced by smithing operations.

Composition of the alloys The composition of the iron–carbon alloys and the presence of phosphorus reveal a certain disparity between the samples (Fig. S3). DUR.6 is a ferritic product (ferrite occupies 74% of the surface), with steel locally around 0.4% C, at the heart of the object. Ghost structures resulting from heterogeneous phosphorous distribution in the ferrite were locally observed (Vega *et al.* 2002). DUR.40 and DUR.48 are comprised of phosphorous iron. The ferrite zones occupy 90 and 60% respectively of the areas studied and include ghost structures that are visible on extensive surfaces of the cross-sections. The last example, DUR.3, is a product

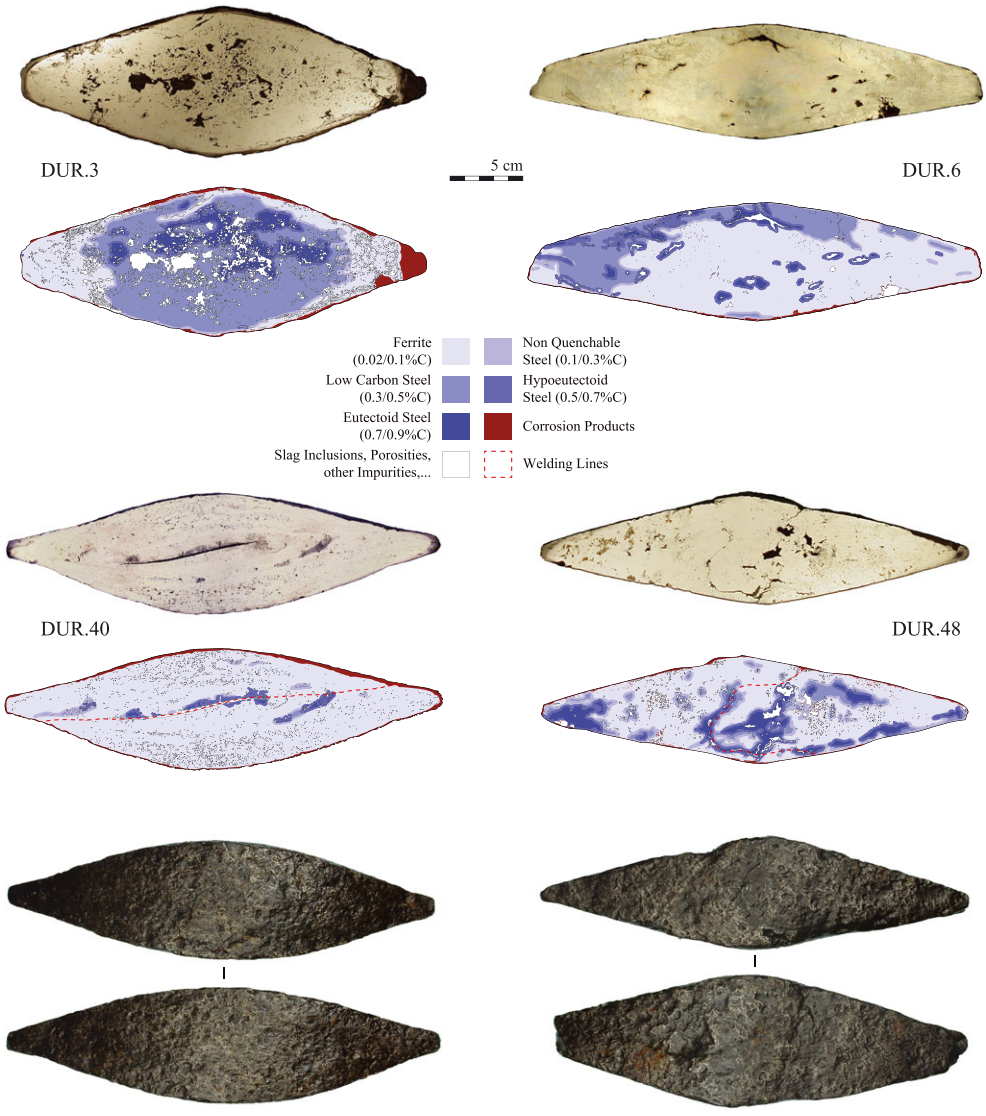

Figure 2 *The presentation of the bipyramidal bars analysed: DUR.3 and DUR.6, photographs of cross-sections, and distribution of carbon; DUR.40 and DUR.48, photographs of faces and cross-sections, and distribution of carbon. [Colour figure can be viewed at wileyonlinelibrary.com]*

mainly made of steel, in the form of ferrite–pearlite zones of 0.2–0.4% C, which occupy 45% of the surface. On nearly one fifth of the surface, the carbon content reaches 0.8%. In the ferrite zones that occupy approximately 35% of the area, ghost structures were only observed occasionally.

Within the four bars, the zones with the highest carbon content lie around the largest pores. These pores promote the ingress of gaseous monoxide (CO) during reduction, penetrating the metallic matrix by carbon diffusion.

Manufacturing techniques Two manufacturing processes can be distinguished (Fig. S3). The first technique concerns DUR.3 and DUR.6 (Fig. 2). These bars were shaped simply by compacting the bloom upon itself. The extremities and surfaces include many small welding lines leading to the surface. These most probably result from metallic excrescences in the initial bloom of metal welding on to themselves.

In DUR.40 and DUR.48, an extended welding line crosses the sections, resulting from the assembly of two consolidated blooms. The DUR.40 section cuts across the welding line perpendicularly (Fig. 2). This is highlighted by a border of inclusions mainly made up of very large wüstite globules. These globules were probably formed by local hot-oxidation of the metal at the time of welding. The DUR.48 cross-section cuts across the welding line almost parallel to its plane (Fig. 2). It is not as accurate, nor of the same quality, as DUR.40. Some zones are perfectly welded, while others are disjointed or have interstitial oxides along the edges.

Welding was only observed on a single longitudinal plane. It is thus not possible to determine whether the two metal masses are totally distinct in three dimensions or correspond, when folded over, to two parts of a single metal mass. This will be determined by chemical analysis of the inclusions.

Summary by semi-product DUR.3 is a bipyramidal bar shaped by simple deformation of a single bloom. The refining quality is poor, with a limited degree of compaction (17% of inclusions remaining). Centimetre-sized pores are visible in the central part of the section studied. It is possible that the deformation of this massive product, mainly made up of steel, was not simple, which would explain that the refining–compacting step was interrupted before it was completed, but after obtaining a product that was regular in appearance.

DUR.6 results from shaping by simple deformation of a single bloom. However, it appears to be much more compact, with only 3% of non-metallic inclusions. It is a ferritic product comprising phosphorus locally, according to the observation of ghost structures present in small proportions. It seems to have been more malleable and more easily compacted than the other bars. It is also possible that the initial bloom was already relatively dense.

DUR.40 is the result of the assembly of two consolidated blooms, each comprised of phosphoric iron. The presence of phosphorus would have engendered specific smithing constraints, including cracking at the usual temperatures (Vega *et al.* 2002). The distribution of the inclusions, which are mainly at the surface, suggests that pre-refining of the two blooms took place before their widest sides were welded together. The result is a homogenous and well-refined bar.

DUR.48 has characteristics that are very similar to those of DUR.40. It was also the result of the welding together of two consolidated blooms, both of which were partly composed of phosphoric iron, but also with extensive steely areas. This is one product for which the refining work was well performed.

Thus, despite the high morphological and metrological homogeneity of this batch of bipyramidal bars, the study of four examples has demonstrated some variability in the nature of their metal masses. Above all, the smithing skills leading to their production seem very different in terms of technical actions. This can be explained by the nature of the initial blooms used to manufacture these bars. The differences in volumes, composition and compaction led to semi-products (trade iron) with different qualities. However, it needs to be stressed that the refining quality and the type of alloy are homogeneous within the same bar, even when it is composed of two metal masses. Finally, the internal structure of these bars showed many indications of incomplete consolidation of the bloom, such as numerous and/or large inclusions

and incompletely agglomerated metallic zones. Thus, in the production process, these objects are much closer to the outcome of the smelting stage than to the final stage in making the objects.

Chemical composition of the slag inclusions

The analysis of SI in the four bipyramidal bars was carried out by looking for the greatest representativeness of the studied zones.

Major element approach Figure 3 illustrates two of the most significant ratios (wt% Al_2O_3/wt% SiO_2 and wt% K_2O/wt% CaO) that can be used to characterize the composition of the inclusions in the bars.

In the DUR.40 bar, the characteristic inclusions in the two metal masses could not be distinguished from each other by their composition (Fig. 3). The strong chemical resemblance between the two parts of the bar shows that DUR.40 is made up of two fragments of a single bloom, produced by a single smelting operation. However, on the assumption of a particularly well-controlled process applied under the same conditions, these two masses could have come from two operations in the same workshop. DUR.40 is characterized by a low content of elements other than Al_2O_3, SiO_2, K_2O and CaO (< 0.5 wt%) and notably by the absence of MnO (Table 1). In contrast, the SI are rich in phosphorus and this confirms the observations made using optical microscopy concerning the presence of ghost structures of phosphorus in the metallic matrix. They have an average P_2O_5 content of 4.2%* and 14.2%**.

Concerning DUR.48, which is also composed of two metallic masses welded together, the inclusions in the two masses show clearly distinct NRC ratios (Fig. 3). These very different signatures are evidence that this bar was made with two blooms produced by two different smelting workshops, and possibly from two distinct ores. For DUR.48–1, the level of MnO is significantly high (1.3%* and 3.4%**), whereas the level of P_2O_5 is low (0.5%* and 1.2%**). DUR.48–2 has both a high level of MgO (3.5%* and 7.42%**) and a level of MnO that is also significantly high (1.4%* and 3%**). The P_2O_5 content of the inclusions corroborates the presence of ghost structures observed by optical microscopy (2.6%* and 6.5%**).

For the two other bipyramidal bars, no welding line was visible by metallography and for each example, a single NRC chemical signature is detectable (Fig. 3). DUR.3 and DUR.6 are both characterized by a high MnO content, of 1.2%* and 3.6%** and 2.4%* and 6.3%** respectively. However, only DUR.3 has a significantly high P_2O_5 level (3.8%* and 10%**), which confirms the difference in their metallographic structure.

Trace element approach Within each part of the bars, once individualized into major elements by their chemical difference, a representative number of SI was selected for LA–ICP–MS investigation (inclusions represented with large dots in Fig. 3). The number of inclusions analysed can vary according to technical constraints, particularly the size of the laser and the sensitivity of the analyser. Thus, in the case of DUR.40 and part 1 of DUR.48, which have large inclusions, we were able to analyse nine inclusions in the former and 10 in the latter. In contrast, the inclusions in the three other bars (DUR.3–DUR.6) and part of one bar (DUR.48–2) are less than 30 μm in size and only three, four and two inclusions, respectively, could be properly analysed.

First, a PCA was carried out on the trace elements in the inclusions, after *log-ratio* normalization. For the first three PCA factors, 92.7% of the variance is represented (Fig. 4 (a)). The figure shows four distinct inclusions groups. The first is formed by the DUR.3 and

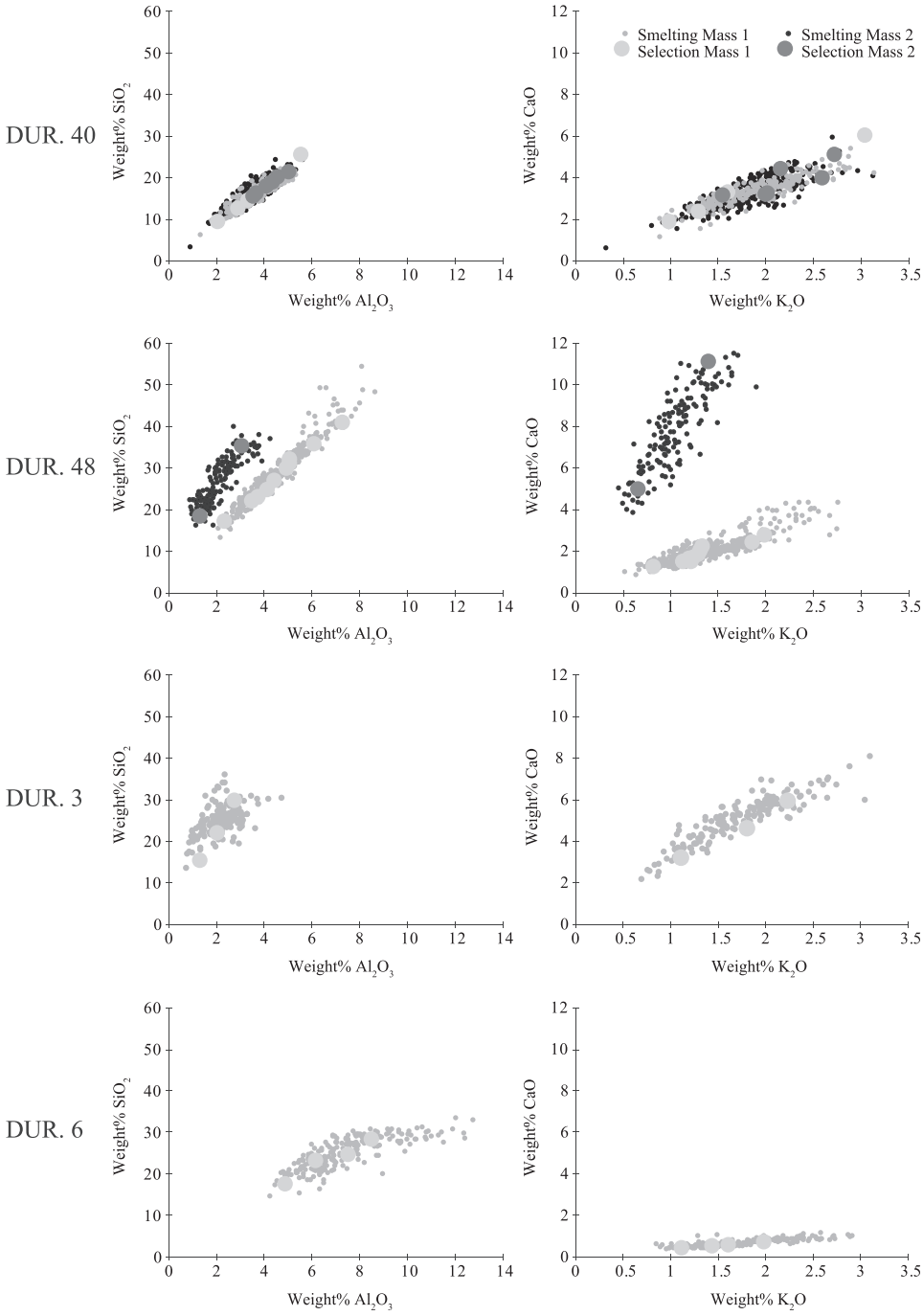

Figure 3 *The Al_2O_3/SiO_2 and K_2O/CaO ratios for the four bipyramidal bars (expressed in wt%): each point represents the content measured for one inclusion. The inclusions shown derive from an initial sorting to eliminate pollution and local concentration effects (Dillmann and L'Héritier 2007; Disser et al. 2014).*

Table 1 *The average values of the major elements obtained by SEM–EDS and analysed (NRC + MnO and P_2O_5) in the five different metal masses: the significant presence of the element is shown in bold type*

Metal mass	*wt% MgO*		*wt% Al_2O_3*		*wt% SiO_2*		*wt% P_2O_5*		*wt% K_2O*		*wt% CaO*		*wt% MnO*	
	*%**	*%***	*%**	*%***	*%**	*%***	*%**	*%***	*%**	*%***	*%**	*%***	*%**	*%***
DUR.40	0.3	0.8	3.6	12.1	16.2	52.5	**4.3**	**14.2**	1.9	6.2	3.3	10.8	0.4	0.8
DUR.48–1	0.5	1.5	4.5	11.8	28.3	72	0.5	1.2	1.4	3.8	2.1	5.4	**1.3**	**3.4**
DUR.48–2	**3.5**	**7.4**	2.2	5.4	27.4	57.2	**2.6**	**6.5**	1.1	2.3	8	16.4	**1.4**	**2.9**
DUR.3	0.3	0.8	2.2	6	24.9	60.9	**3.8**	**10**	1.8	4.5	5	13.1	**1.2**	**3.6**
DUR.6	0.4	1.1	7.4	18.9	25	64.5	0.5	1.1	1.7	4.3	0.7	1.6	**2.4**	**6.3**

%*, Mean surface-weighted composition of the group of inclusions.

%**, Mean surface-weighted composition normalized to 100% without FeO.

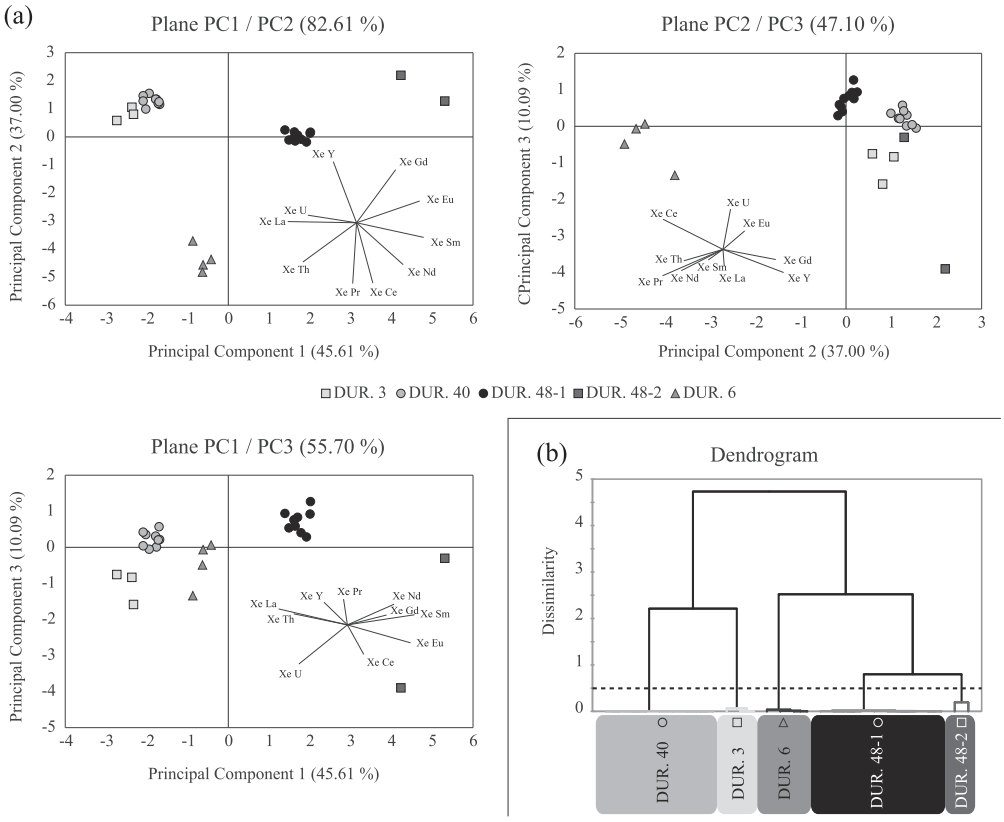

Figure 4 *Multivariate statistical analyses performed on X_E of the four bipyramidal bars. (a) The projection of the highest variance (principal components 1, 2 and 3) of the principal component analysis; (b) a dendrogram representing the results of the hierarchical ascending classification.*

DUR.40 masses and the three others by the three individuals DUR.6, DUR.48–1 and DUR.48–2. The internal differences in each individual metallic mass (differences between the chemical signatures of each inclusion in the same mass) seem smaller than the differences that exist between the five metallic masses. However, on these representations, the signatures of the DUR.3 and DUR.40 masses appear to be similar.

HAC carried out using the X_E data allows the classification of the inclusions and shows a greater dissimilarity between DUR.40 and DUR.3 than between the two metallic masses making up DUR.48 (DUR.48–1 and 48–2; Fig. 4 (b)). It is therefore impossible to link these two masses to a common origin, especially if the difference observed at the highest level of the major elements is taken into account, and in particular because a significant MnO level is found in the inclusions of DUR.3, and because it is virtually absent in the DUR.40 inclusions.

The results from both major and trace elements analyses converge towards the existence of five metal masses of different origins. This observation sanctions future initial comparisons by major elements, thus avoiding the higher costs of trace element analyses.

Results of radiocarbon dating

Following the approach described above, it was possible to date each bar after sampling the zones in the cross-sections that locally contained sufficient carbon (> 0.02 wt% C). For the objects made of two metal masses, we took care to sample only one of the two masses.

Table S2 shows the results of dating carried out for each of the bipyramidal bars. The age distributions and the results of combinations of two measurements obtained at the scale of each dated bipyramidal bars are shown in Figure 5. Most of the calibrated ages are consistently within the interval determined by a 2-sigma uncertainty and grouped around the plateau of the early Iron Age. The high consistency between the dates obtained for a single object confirms their probability. Only the dating of DUR.3 produced two age distributions that do not overlap within the 2-sigma interval, one situated around 900–800 cal BC, and the other on the Hallstatt plateau (756–412 cal BC). For both DUR.3 samples, the amount of carbon extracted was sufficiently high (> 1 mg) and the analysis of $\delta^{13}C$ is consistent enough to attest to the accuracy of the results. The shift towards older dates in the radiocarbon measurements of DUR3–2 could be compatible with an ‘old wood’ effect. Another possible explanation is that the presence of a plateau on the calibration curve around 2700 BP would have a tendency to lengthen the age density towards the older dates, and would not allow precise calibration.

Nevertheless, dating allowed all these objects to be attributed to the early Iron Age. Given that the calibration curve for the period considered shows a plateau between -800 and -420 cal BC, it is impossible to establish a more accurate date. However, the results of absolute dating allow us to exclude the attribution of this deposit to the later Iron Age or the Roman period.

DISCUSSION

The batch of 51 bipyramidal bars discovered at Durrenentzen shows a high degree of morphological and metrological homogeneity, which has raised two main questions. Is this homogeneity also found internally (microscopic and chemical properties)? What information about metal circulation can be obtained from the properties of these semi-products (trade iron)?

Even if the refining and the nature of the alloy are homogeneous within a single bar whether it is made up of one or two different metal masses, the metallographic analysis shows significant internal differences between the four bipyramidal bars. These differences concern, first, the

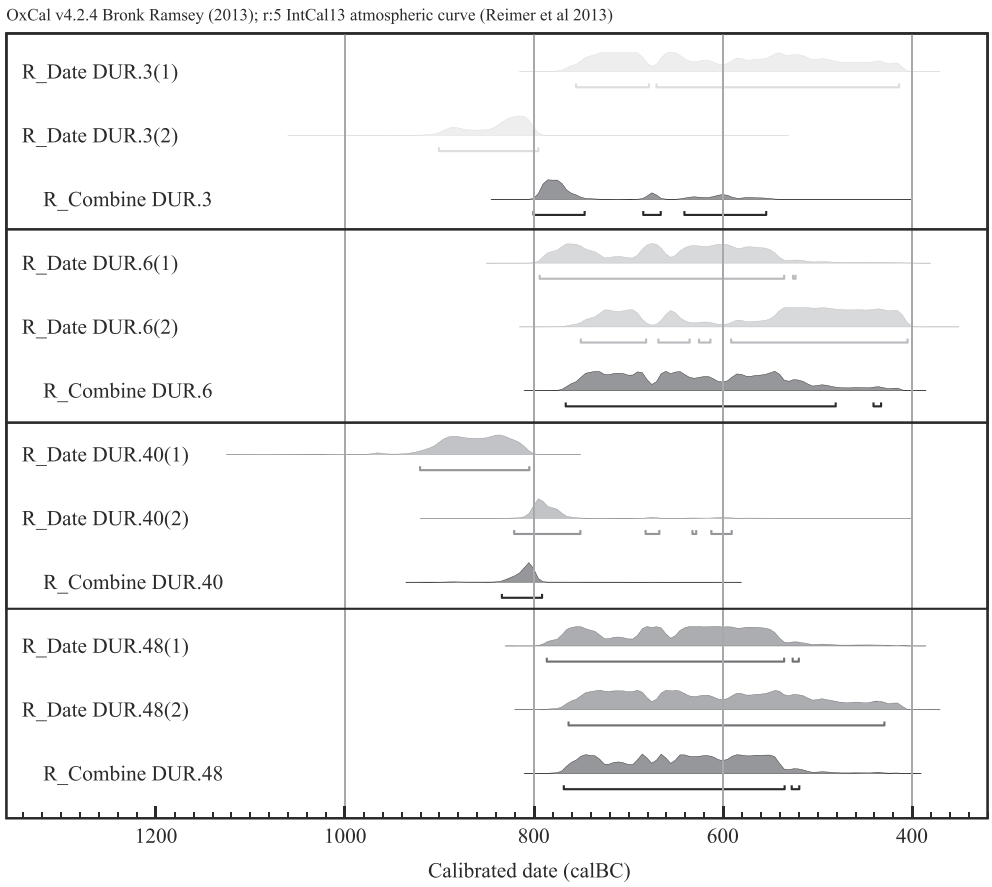

Figure 5 *The age distributions (95.4% probability) of the two ^{14}C measurements obtained for each of the four bars and combinations (R-combine) of the two measurements.*

degree of refining, which is highly variable from one object to another and, second, the manufacturing techniques, with two individual specimens resulting from the welding together of different consolidated blooms and two others each made from a single bloom. Finally, they concern the chemical composition of the metal, with three distinct alloys. Two bars are made of phosphoric iron, while another is mainly ferritic and the last one is mainly composed of steel. These structural differences impart specific mechanical, ductility and resistance properties to each of the semi-products. This heterogeneity between the semi-products is also observed in the chemical signatures. The chemical analysis of the inclusions of six metal masses reveals the existence of five different chemical signatures.

The multiple chemical signatures within the same object suggest a complex exchange system, as shown from the analysis of the socket bars dating from the late Iron Age (Bauvais and Fluzin 2006; Berranger *et al.* 2007). This system is characterized by the segmentation of the production (into smelting activities, manufacturing of semi-products and confection of objects) also documented in workshops of the same period (Bauvais 2008; Berranger 2014). The results of this study allow the specialization between craftsmen to be dated to much earlier periods, although it is barely perceptible from the study of contemporary workshops alone.

Radiocarbon dating allows this deposit to be dated to an early period in the development of iron metallurgy, that of the Hallstatt and early La Tène periods. This confirms the dating already obtained for micro wood-charcoal conserved in the pores of two bipyramidal bars from a deposit of 24 bars of this form (Nottonville, Eure et Loire, France; Berranger 2014). So far, the sites yielding bipyramidals and dated by their archaeological contexts are mainly associated with the late Hallstatt (HaD) and early La Tène (LTA) (Berranger 2014). Our study results thus provide additional arguments in favour of earlier dating of these bipyramidal bars. Due to the interdisciplinary study on the Durrenentzen iron bars, we can now attribute their technical characteristics to the cultural context of the later early Iron Age.

The deposit, made up of just over 308 kg of refined iron, reveals the circulation of considerable quantities of metal, even though finished objects for this period are only known in small amounts at consumer sites. Of about 15 aristocratic Hallstatt D sites in which metal workshops have recently been studied, the vast residential complex of Heuneburg (Germany) is the only one that stands out for its large quantities of iron objects, which nevertheless do not weigh more than 12 kg (Dubreucq 2013). Most other settlements have not delivered more than 1 kg of iron.

This study reveals the assembly of metal masses of distinct origins within a single bar. This shows that the raw material circulated in the form of blooms, barely consolidated if at all, directly from the smelting workshops. This analysis, already put forward by Gaspard Pagès for the Gallo-Roman bars from Saintes-Maries-de-la-Mer (Pagès *et al.* 2011), confirms that even in the early Iron Age, metal circulated in its raw form and was not necessarily compacted at the smelting site. The blooms found at Bourges and dated to the early La Tène (LTA) provide excellent additional evidence (Fournier and Milcent 2007) that agrees with the observations made for this study. However, this concerns a form of iron exchange that has barely been demonstrated, because of the almost complete lack of blooms from this period. The diversity of the chemical signatures noted during this study could indicate that the craftsmen acquired their blooms through various trading networks. The final shaping of these products could thus have been effected in a forge or a group of forges working to a particular metrological standard. This is the deduction we have made from the overall morphological homogeneity of the batch, together with the existence of variations in detail.

Because some bipyramidal bars were made from several different blooms, we conclude that the consolidated bloom metal was acquired and then reworked so as to yield bars of a standard size and shape. This could explain the welding flaws observed on some of the bars. The bipyramidal (or fish) shape is one shape that results ‘naturally’ from the consolidation or compaction of a raw bloom (Thouvenin 1984). Bipyramidal bars from other periods have a similar morphology, such as the Neo-Assyrian fish-shaped bars from Khorsabad, Susa or Nimrud (Pleiner 2006, 25), or the bipyramidal bars from the medieval wrecks discovered off the Carmel coast (Galili *et al.* 2015). The presence in these wrecks of blooms in differing stages of consolidation clearly shows the link between the bipyramidal shape and the consolidation of the blooms. The similar size and shape of the bipyramidal bars examined in the present study, and the fact that some were made by welding together more than one consolidated bloom, shows that this particular size and shape was a chosen standard rather than a technological necessity.

This conformance to common standards is generally well known in the same periods for the manufacture of finished objects, such as fibulae, some of which were mass-produced (Carrara *et al.* 2013; Dubreucq 2013). This is even more noticeable when ceramics are considered. In the Hallstatt region, it was during the Hallstatt D2/D3-La Tène A that the new system of throwing ceramic pots on a wheel was adopted and began to spread. In earlier periods, these wheel-thrown

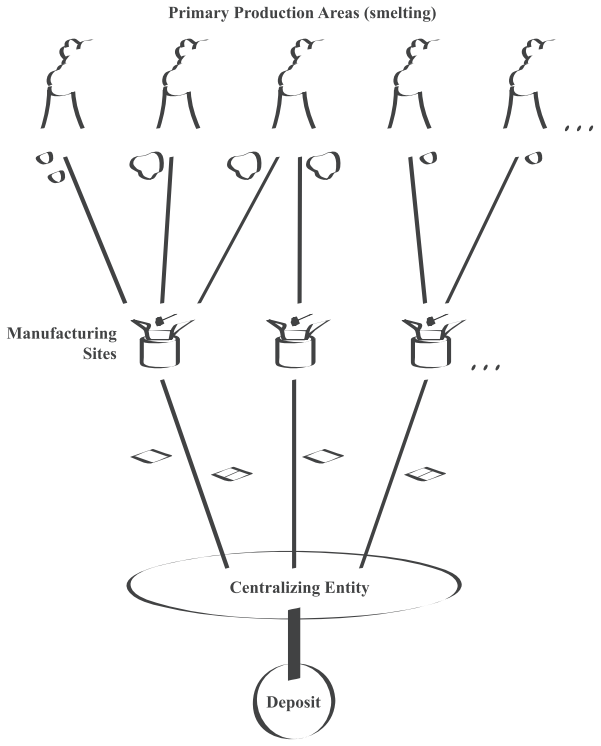

Several production areas were characterized by:
- several technical traditions
  * blooms of different size
  * heterogeneous iron/carbon alloys
  * variable presence of phosphorus
  * initial compaction possibly different
- different geochemical signatures
  * different geological resources

Possible commercial intermediaries:
A site can acquire blooms from several sites of primary production (smelting)

Several manufacturing sites are characterized by:
- standards of shared morphologies
  * bipyramidal form of semi-products despite a shaping by welding of two masses
- common metrological standards
  * almost identical weights and sizes
  * breakage of tips to conform to the standard
- slight variations of shaping
  * central edges more or less marked
  * lateral edges more or less rectilinear

A centralizing entity is characterized by a power sufficiently strong to:
- centralize more than 300 kg of iron
  * low quantity of iron are found in the contemporary residential sites
  * the iron is almost exclusively intended for social elites (ornaments and arms)
- unite several manufacturing sites around a metrological standard
  * possible setting up of a standard
- remove such a mass of metal from the economic circuit
  * demonstrate power, ritual practice etc.

Figure 6 *A theoretical model of the relationships between the different contributors involved in creating the Durrenentzen deposit.*

pots seem to have been made in specialized workshops, located next to the princely sites (Augier *et al.* 2013). The same link between the distribution of bipyramidal bars and the distribution of these centres of power has already been noted (Berranger and Fluzin 2012). The Durrenentzen deposit is located only 10 km from the Breisach 'Münsterhügel', a princely site of the late Hallstatt and early La Tène periods (HaD/LTA) (Balzer 2009). This case study thus provides new material relative to the importance of the elites in the dissemination of products and skills, but also allows a better assessment of their role in driving the emergence of new specializations and structured craft industries.

CONCLUSIONS

The study of this exceptional deposit has laid the foundations for a more general analysis that significantly changes perceptions of the iron economy in the early Iron Age.

The circulation of iron during the early times of its use in the North of Europe has sometimes been neglected and sometimes exaggerated, but is documented here in a new way for the first time. Our study proposes a vision of the 'history' of some Hallstatt bipyramidal iron bars (semi-products), from their genesis in the form of a raw bloom up to their manufacture and their exit from the economic circuits. The new archaeometric approaches used here have allowed us not only to assign the deposit to the Hallstatt period (^{14}C dating of the carbon in steels), but also to demonstrate the composite character of some bars and the heterogeneous origins of the deposit

as a whole. A theoretical model of a complex economy can thus be outlined, which brings many factors into play at different technical levels and degrees of involvement (Fig. 6). The nature of the relationships between these players seems more complex than a simple direct relationship between producer and consumer, and the amount of metal in circulation seems much larger than the residential sites of this period had led us to assume.

This initial foundation, of the order of a theoretical model, opens up new perspectives for the interpretation of the iron economy during the Iron Ages. The interdisciplinary approach developed within the LMC/LAPA-IRAMAT and applied to this set of artefacts should now be extended to other deposits of the North Alpine complex to consolidate these initial conclusions.

Finally, one essential step in the approach remains to be developed, which is a true provenance study (Leroy *et al.* 2012; Charlton 2015; Disser *et al.* 2016). A geochemical database (major elements, traces and osmium isotopes) of iron production areas in the north of France and the south of Germany is currently being developed. This incorporates several studies by the LMC/LAPA-IRAMAT (Bauvais *et al.* 2011, 2015; Berranger 2015; see also Ph.D. theses by A. Disser and N. Zaour). The next step will be to compare these initial results with the potential production areas, which will finally allow production centres to be linked to consumption centres. It will add to this theoretical model the geo-economic and geopolitical relationships that are crucial to an overall understanding of the protohistoric iron economy.

ACKNOWLEDGEMENTS

We wish to thank Suzanne Plouin, curator of the Biesheim Museum, for giving us access to the bars. We also thank the Crelier SA Company, which kindly undertook the water-jet cutting of the objects. We are grateful to the LMC14 (LSCE) team for making the radiocarbon measurements on ARTEMIS and to our colleagues at the CEB–IRAMAT for their welcome and their help with the LA–ICP–MS.

REFERENCES

Augier, L., Balzer, I., Bardel, D., Deffressigne, S., Bertrand, E., Fleischer, F., Hopert-Hagmann, S., Lndolt, M., Mennessier-Jouannet, C., Mège, C., Roth-Zehner, M., Saurel, M., Tappert, C., Thierrin-Michael, G., and Tikonoff, N., 2013, La céramique faconnée au tour: témoin privilégié de la diffusion des techniques au Hallstatt D2-D3 et à La Tène A-B1, in *L'âge du Fer en Aquitaine et sur ses marges: mobilité des hommes, diffusion des idées, circulation des biens dans l'espace européen de l'âge du Fer* (eds. A. Colin and F. Verdin), 563–94, Aquitania, supplément 30, Fédération Aquitania, Bordeaux.

Balzer, I. (ed.), 2009, Chronologisch–chorologische Untersuchung des späthallstatt- und frühlatènezeitlichen 'Fürstensitzes' auf dem Münsterberg von Breisach (Grabungen 1980–1986), Materialhefte zur Archäologie in Baden-Württemberg, Konrad-Theiss Verlag, Stuttgart.

Bauvais, S., 2008, Du prestige à la proto-industrie: évolution des pratiques sidérurgiques au second âge du Fer dans le nord du Bassin parisien, *The Arkeotek Journal*, **2**(4).

Bauvais, S., and Fluzin, P., 2006, Réflexion sur l'organisation technico-sociale des activités de forge à La Tène finale dans l'Aisne (02), *Revue d'Archéométrie*, **30**, 25–43.

Bauvais, S., Schwab, R., Brauns, M., and Dillmann, P., 2011, Circulation of iron products in the Iron Age of eastern France and southern Germany: multidisciplinary and methodological approaches towards the provenance of ancient iron, *Metalla Sonderheft*, **4**, 95–6.

Bauvais, S., Dillmann, P., Disser, A., Leroy, S., Berranger, M., Pagès, G., and Vega, E., 2015, Circulation of iron products in the Iron-Age of eastern France and southern Germany: multidisciplinary and methodological approaches towards the provenance of ancient iron (CIPIA), Rapport final de programme ANR–DFG, Agence Nationale de la Recherche, Paris/LAPA-IRAMAT, Saclay.

Berranger, M., 2014, Le fer, entre matière première et moyen d'échange, en France du VII^{e} au I^{er} s. av. J.-C.: approches interdisciplinaires, Art, Archéologie et Patrimoine, Editions Universitaires de Dijon, Dijon.

Berranger, M. (ed.), 2015, La sidérurgie en Bourgogne et en Franche-Comté avant le haut fourneau: organisation et circulation des productions, Projet collectif de recherché, LMC–IRAMAT, Belfort/Service Régional de l'Archéologie Bourgogne-Franche-Comté, Besançon.

Berranger, M., and Fluzin, P., 2012, From raw iron to semi-product: quality and circulation of materials during the Iron Age in France, *Archaeometry*, **54**, 664–84.

Berranger, M., Bauvais, S., and Fluzin, P., 2007, 'Socket bars': multidisciplinary results (archaeology and archaeometry) on a specific iron semi-product in north of France, in *Archaeometallurgy in Europe 2007, international conference in Grado–Aquilea (Italy), 2007*, electronic publication.

Biellmann, P., 1986, Les lingôts de fer de Durrenentzen, *Annuaire de la société d'histoire de la Hardt et du Ried*, **1**, 11–18.

Carrara, S., Dubreucq, É., and Pescher, B., 2013, La fabrication des fibules à timbale comme marqueur des contacts et des transferts technologiques au cours du Ha D-LT A1: nouvelles données d'après les sites de Bourges, Lyon et Plombières-les-Dijon, in *L'âge du Fer en Aquitaine et sur ses marges: mobilité des hommes, diffusion des idées, circulation des biens dans l'espace européen de l'âge du Fer* (eds. A. Colin and F. Verdin), 595–608, Aquitania, supplément 30, Fédération Aquitania, Bordeaux.

Charlton, M. F., 2015, The last frontier in 'sourcing': the hopes, constraints and future for iron provenance research, *Journal of Archaeological Science*, **56**, 210–20.

Coustures, M. P., Béziat, D., Tollon, F., Domergue, C., Long, L., and Rebiscoul, A., 2003, The use of trace element analysis of entrapped slag inclusions to establish ore – bar iron links: examples from two Gallo-Roman iron-making sites in France (Les Martys, Montagne Noire, and Les Ferrys, Loiret), *Archaeometry*, **45**, 599–613.

Desaulty, A.-M., Dillmann, P., L'Héritier, M., Mariet, C., Gratuze, B., Joron, J.-L., and Fluzin, P., 2009, Does it come from the Pays de Bray? Examination of an origin hypothesis for the ferrous reinforcements used in French medieval churches using major and trace element analyses, *Journal of Archaeological Science*, **36**(10), 2445–62.

Dillmann, P., and L'Héritier, M., 2007, Slag inclusion analyses for studying ferrous alloys employed in French medieval buildings: supply of materials and diffusion of smelting processes, *Journal of Archaeological Science*, **34**(11), 1810–23.

Disser, A., 2014, *Production et circulation du fer en Lorraine* (VIe s. av. J.-C. - XVe s. ap. J.-C.), Ph.D. thesis, Université de Technologie de Belfort-Montbéliard/Université de Franche-Comté, Belfort, 1038.

Disser, A., Dillmann, P., Leroy, M., L'Héritier, M., Bauvais, S., and Fluzin, P., 2016, Iron supply for the building of Metz cathedral: new methodological development for provenance studies and historical considerations, *Archaeometry*, DOI: 10.1111/arcm.12265.

Disser, A., Dillmann, P., Bourgain, C., L'Héritier, M., Vega, E., Bauvais, S., and Leroy, M., 2014, Iron reinforcements in Beauvais and Metz Cathedrals: from bloomery or finery? The use of logistic regression for differentiating smelting processes, *Journal of Archaeological Science*, **42**(1), 315–33.

Dubreucq, É., 2013, Métal des premiers celtes: productions métalliques sur les habitats dans les provinces du Hallstatt centre-occidental, Arts, Archéologie et Patrimoine, Editions Universitaires de Dijon, Dijon.

Fluzin, P., 2002, La chaîne-opératoire en sidérurgie: matériaux archéologiques et procédés. Apport des études métallographiques, in *Aux origines de la métallurgie du fer en Afrique: une ancienneté méconnue* (ed. H. Bocoum), 59–91, Mémoire des peuples, UNESCO, Paris.

Fluzin, P., Bauvais, S., Berranger, M., Pagès, G., and Dillmann, P., 2011, The multidisciplinary approach (archaeology and archaeometry) to bloomsmithing activities in France: examples of results from the last twenty years, in *The archaeometallurgy of iron—recent developments in archaeological and scientific research* (eds. J. Hosek, H. Cleere, and L. Mihok), 223–36, Institute of Archaeology of the ASCR, Prague.

Fournier, L., and Milcent, P.-Y., 2007, Actualité des recherches sur l'économie du fer protohistorique dans la région Centre, in *L'économie du fer protohistorique: de la production à la consommation du métal* (ed. P.-Y. Milcent), 85–105, Aquitania, supplément 14/2, Fédération Aquitania, Bordeaux.

Galili, E., Bauvais, S., Rosen, B., and Dillmann, P., 2015, Cargoes of iron semi-products recovered from shipwrecks off the Carmel coast, *Israel, Archaeometry*, **57**, 505–35.

Kleemann, O., 1981, Les lingots de fer bipyramidaux courts et épais: les lingots du type Colmar, *Revue Archéologique de l'Est*, **32**, 109–19.

Leroy, S., Hendrickson, M., Delqué-Kolic, E., Vega, E., and Dillmann, P., 2015a, First direct dating for the construction and modification of the Baphuon Temple Mountain in Angkor, *Cambodia, PLoS ONE*, **10**, e0141052.

Leroy, S., L'Héritier, L., Delqué-Kolic, E., Dumoulin, J.-P., Moreau, C., and Dillmann, P., 2015b, Consolidation or initial design? Radiocarbon dating of ancient iron alloys sheds light on the reinforcements of French gothic cathedrals, *Journal of Archaeological Science*, **53**, 190–201.

Leroy, S., Cohen, S. X., Verna, C., Gratuze, B., Téreygeol, F., Fluzin, P., Bertrand, L., and Dillmann, P., 2012, The medieval iron market in Ariège (France): multidisciplinary analytical approach and multivariate analyses, *Journal of Archaeological Science*, **39**(4), 1080–93.

Pagès, G., Dillmann, P., Fluzin, P., and Long, L., 2011, A study of the Roman iron bars of Saintes-Maries-de-la-Mer (Bouches-du-Rhône, France): a proposal for a comprehensive metallographic approach, *Journal of Archaeological Science*, **38**(6), 1234–52.

Pleiner, R., 2006, *Iron in archaeology: early European blacksmiths*, Archeologický ústav AV ČR, Prague.

Pleiner, R., and Bjorkman, J., 1974, The Assyrian Iron Age: the history of iron in the Assyrian civilization, *Proceedings of the American Philosophical Society*, **118**(3), 283–313.

Ramsey, C. B., and Lee, S., 2013, Recent and planned developments of the program OxCal, *Radiocarbon*, **55**, 3–4.

Reimer, P. J., Bard, E., Bayliss, A., Beck, J. W., Blackwell, P. G., Bronk Ramsey, C., Buck, C. E., Cheng, H., Edwards, R. L., Friedrich, M., Grootes, P. M., Guilderson, T. P., Haflidason, H., Hajdas, I., Hatté, C., Heaton, T. J., Hoffmann, D. L., Hogg, A. G., Hughen, K. A., Kaiser, K. F., Kromer, B., Manning, S. W., Niu, M., Reimer, R. W., Richards, D. A., Scott, E. M., Southon, J. R., Staff, R. A., Turney, C. S. M., and van der Plicht, J., 2013, IntCal13 and Marine13 radiocarbon age calibration curves 0–50,000 years cal BP, *Radiocarbon*, **55**(4), 1869–87.

Senn, M., Kraack, M., Flisch, A., Wichser, A., and Obrist, M., 2014, An aspect of the Celtic iron trade: the 'Spitzbarren'. The deposit from Bellmund (canton Bern, Switzerland), in *Early iron in Europe* (eds. B. Cech and T. Rehren), 147–60, Monographie Instrumentum, 50, Editions Monique Mergoil, Montagnac.

Thouvenin, A., 1984, Lingots de fer gaulois et techniques de forge, *Revue archéologique de l'est et du centre est*, **25**(3–4), 368–72.

Vega, E., Dillmann, P., and Fluzin, P., 2002, Contribution à l'étude du fer phosphoreux en sidérurgie ancienne, *La Revue d'Archéométrie*, **26**, 197–208.

Zaour, N., in progress, *La métallurgie du fer en Normandie de l'âge du Fer au moyen-âge: approches interdisciplinaires, archéologique et archéométrique*, Ph.D. thesis, Université de Technologie de Belfort-Montbéliard/Univestité de Franche-Comté, Belfort.

SUPPORTING INFORMATION

Additional Supporting Information may be found online in the supporting information tab for this article.

Table S1. Summary of the metallographic characteristics of the bars.
Table S2. Results of ^{14}C dating performed on the Durrenentzen iron bars. Calibration was done with Oxcal 4.2.4 software (Ramsey, 2013), which uses the IntCal 13 calibration curve (Reimer et al., 2013).
Table S3. Composition in major elements of each slag inclusion selected for full chemical analysis.
Table S4. Composition in trace elements and rare earth elements of each slag inclusion selected for full chemical analysis.
Figure S1. Metrological characteristics of the Durrenentzen iron bars.
Figure S2. Typo-morphological classification of the Durrenentzen iron bars. The first two levels of description (central and lateral edges) seem to correspond to differences in the "technical traditions" of the finishing techniques. The third level (symmetrical base, off-cantered, thickset) appears to reflect poorly-mastered variations in shaping.
Figure S3. Microphotographs showing inclusion quality, chemical composition and manufacturing techniques demonstrated by metallographic analysis of the bars.

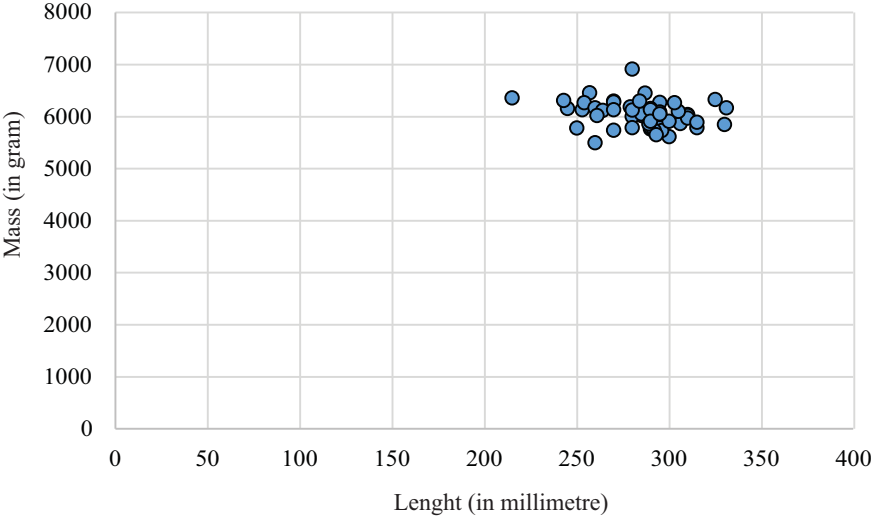
8000
7000
6000
5000
4000
3000
2000
1000
0
Mass (in gram)
0
50
100
150
200
250
300
350
400
Lenght (in millimetre)

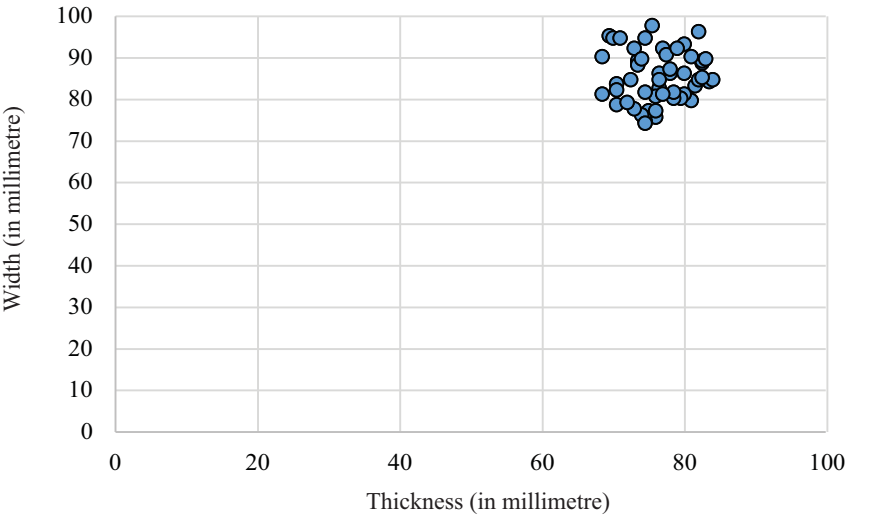
100
90
80
70
60
50
40
30
20
10
0
Width (in millimetre)
0
20
40
60
80
100
Thickness (in millimetre)

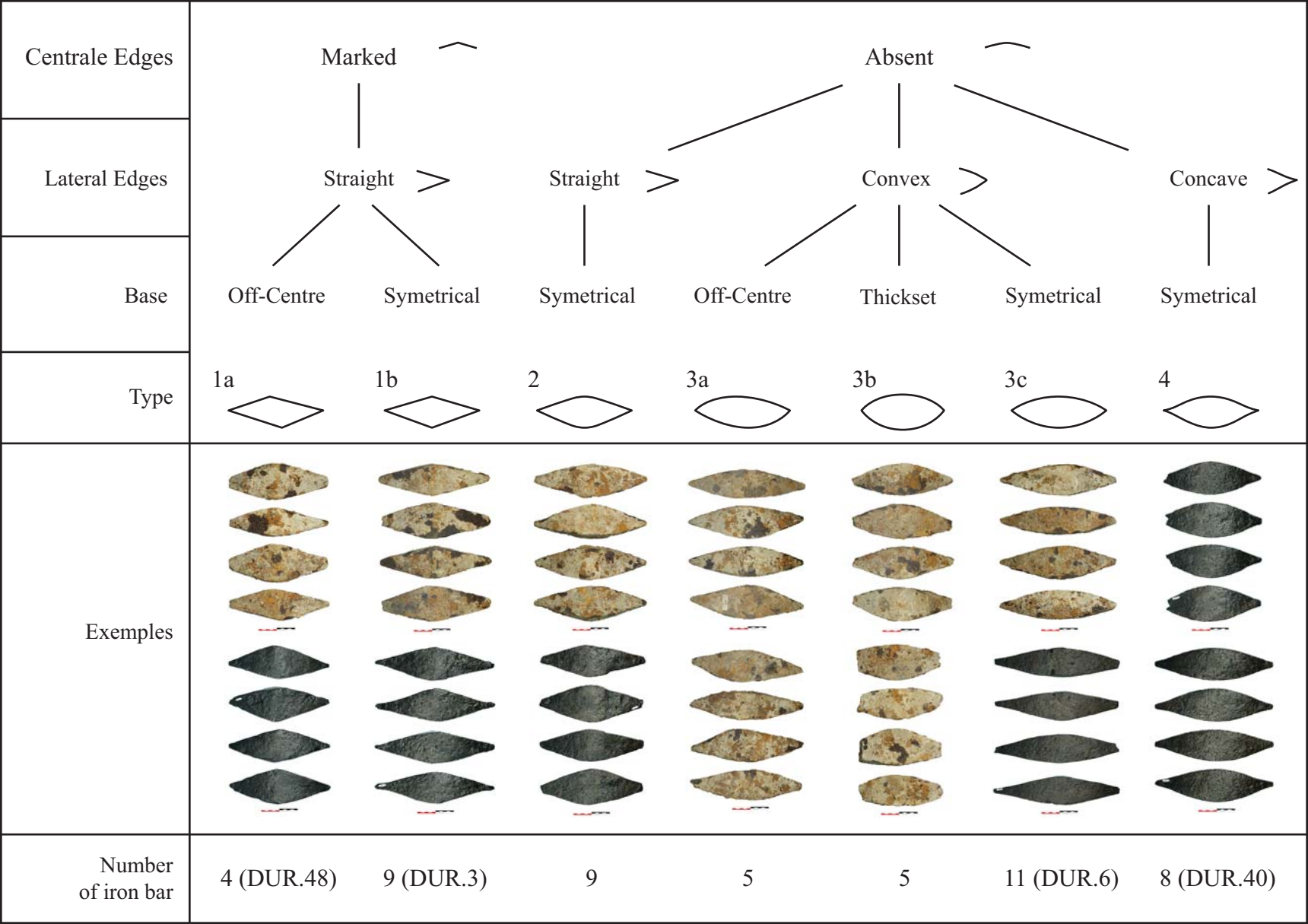
Centrale Edges
Marked
Absent
Lateral Edges
Straight
Straight
Convex
Concave
Base
Off-Centre
Symetrical
Symetrical
Off-Centre
Thickset
Symetrical
Symetrical
Type
1a
1b
2
3a
3b
3c
4
Exemples
Number of iron bar
4 (DUR.48)
9 (DUR.3)
9
5
5
11 (DUR.6)
8 (DUR.40)

Inclusionary Cleanliness

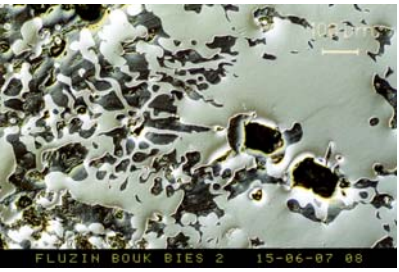

DUR.48: Strong density of inclusions. Metal incompletely agglomerated.

DUR.40: Mainly siliceous inclusions.

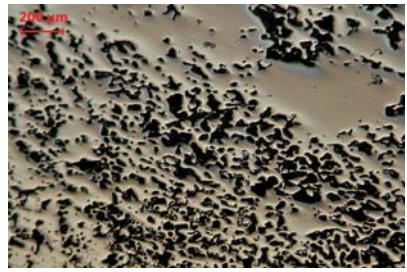

DUR.3: Strong concentration of porosities with round outlines.

Composition of alloys

DUR.40: Neumann banding (shock-induced strain lines) in equiaxed ferrite grains.

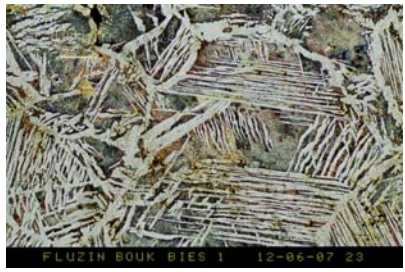

DUR.40: 0.4-0.5%C steel (acicular ferrite, Widmanstätten structure).

DUR.6: 0.6-0.7%C steel.

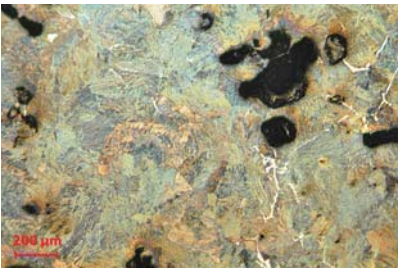

DUR.3: 0.8%C steel (eutectoid).

DUR.48: 0.9%C steel (hypereutectoid).

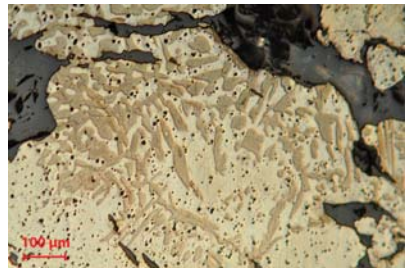

DUR.6: Ghost structure resulting from variations in phosphorus distribution.

Manufacturing techniques

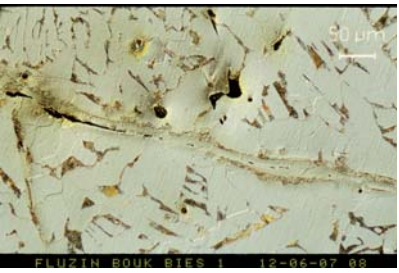

DUR.40: A near perfect weld between two pieces of low carbon iron with about 0.1%C.

DUR.40: Local debonding of the ferrite, in connection with hot oxidation.

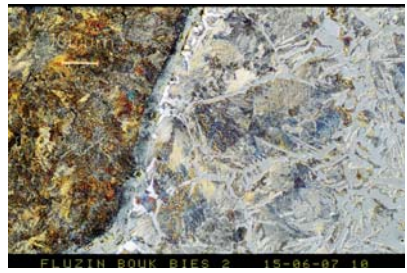

DUR.48: Perfectly realized welding between steels of 0.8%C and 0.5%C.

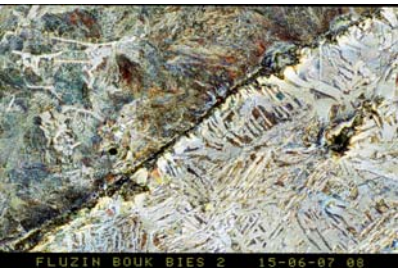

DUR.48: A clearly marked weld (with a line of slag) between steels of 0.8% and 0.4%C.

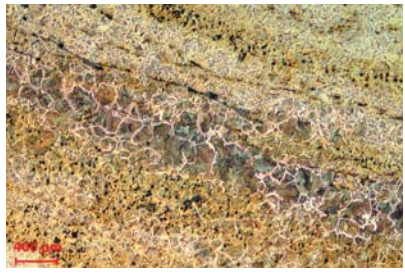

DUR.6: Banded variable steel/low carbon structure.

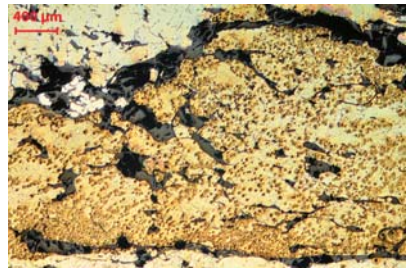

DUR.6: Internal weldings of a metal mass compacted on itself.

Bipyramidal bar	Inclusionary Cleanliness	Iron/Carbon Alloy			Ghost Structures of Phosphorus	Nombre of Metal Mass
		from ferrite to 0.2%C	from 0.2 to 0.6%C	from 0.7 to 0.8%C		
DUR.3	17%	36%	45%	19%	Local	1
DUR.6	3%	74%	20%	6%	Local	1
DUR.40	4%	90%	6%	4%	Extended	2
DUR.48	7%	66%	10%	24%	Extended	2

Supplementary material Table S1

Sample	Lab Code (SacA)	Amount of extracted carbon (mg)	$d^{13}C$ (‰)	pMC	Radiocarbon Age BP +/- (1σ)	Calibrated Age (95.4 %)
DUR.40(1)	26691	1.57	-30.4	71.35 ± 0.32	2712 ± 36	923-804 BC
DUR.40(2)	26692	1.5	-27.6	72.46 ± 0.28	2588 ± 31	821-594 BC
DUR.48(1)	26693	1.2	-23.9	73.26 ± 0.28	2499 ± 31	786-515 BC
DUR.48(2)	26694	0.87	-28.9	73.58 ± 0.30	2465 ± 33	761-414 BC
DUR.3(1)	26695	1.45	-18.3	73.65 ± 0.29	2457 ± 32	756-412 BC
DUR.3(2)	26696	1.42	-22.8	71.71 ± 0.33	2671 ± 37	900-796 BC
DUR.6(1)	26697	0.3	-37.6	73.14 ± 0.33	2513 ± 36	792-521 BC
DUR.6(2)	26698	0.86	-29.9	73.86 ± 0.30	2434 ± 33	752-404 BC

Supplementary material Table S2

Supplementary material Table S3

Metal mass	Dur 3	Dur 3	Dur 3	DUR.40-1	DUR.40-1	DUR.40-1	DUR.40-2	DUR.40-2	DUR.40-2	DUR.40-2	DUR.40-2	DUR.40-2
Inclusion	1	2	3	1	2	3	4	5	6	7	8	9
Major elements in oxide weight %												
Na_2O	0.3	0.4	0.7	0.0	0.2	0.0	0.3	0.3	0.1	0.5	0.5	0.2
MgO	0.5	0.4	0.2	0.1	0.4	0.2	0.3	0.4	0.3	0.2	0.4	0.2
Al_2O_3	2.7	2.0	1.3	2.9	5.5	3.3	5.0	3.5	4.3	3.7	4.6	4.1
SiO_2	29.8	21.9	15.3	12.4	25.5	14.6	21.2	15.4	18.7	16.1	20.0	17.8
P_2O_5	5.0	3.4	1.7	2.8	5.7	3.6	6.5	3.6	7.0	3.6	5.3	4.3
SO_2	0.4	0.3	0.2	0.2	0.2	0.2	0.2	0.4	0.2	0.2	0.4	0.2
ClO	0.2	0.3	0.1	0.1	0.2	0.1	0.1	0.3	0.2	0.1	0.3	0.1
K_2O	2.2	1.8	1.1	1.3	3.1	1.6	2.7	2.0	2.2	1.6	2.6	2.0
CaO	5.9	4.6	3.2	2.3	6.0	3.3	5.1	3.2	4.4	3.2	4.0	3.2
TiO_2	0.1	0.6	0.6	0.2	0.3	0.2	0.3	0.3	0.2	0.3	0.3	0.3
V_2O_5	0.0	0.8	0.4	0.1	0.4	0.1	0.0	0.0	0.2	0.2	0.2	0.1
MnO	1.7	1.0	0.8	0.4	0.6	0.2	0.3	0.0	0.2	0.4	0.2	0.2
FeO	51.1	62.6	74.6	77.1	51.9	72.7	57.8	70.6	62.0	70.1	61.0	67.5

Metal mass	Dur 48-1	Dur 48-1	Dur 48-1	Dur 48-1	Dur 48-1	Dur 48-1	Dur 48-1	Dur 48-1	Dur 48-1	Dur 48-1	Dur 48-2	Dur 48-2	Dur 6	Dur 6	Dur 6	Dur 6
Inclusion	1	2	3	4	5	6	7	8	9	10	1	2	1	2	3	4
Major elements in oxide weight %																
Na_2O	0.0	0.0	0.0	0.0	0.1	0.2	0.0	0.0	0.0	0.2	0.2	0.6	0.1	0.2	0.1	0.2
MgO	0.3	0.3	0.3	0.7	0.4	0.2	0.6	0.6	0.5	1.1	3.3	4.3	0.5	0.3	0.3	0.3
Al_2O_3	2.3	3.5	4.1	6.1	3.7	4.4	4.9	5.0	5.1	7.3	1.3	3.0	8.5	7.5	4.9	6.1
SiO_2	16.9	21.8	24.5	35.6	22.9	26.7	29.7	31.9	30.9	40.7	18.2	35.1	28.3	24.7	17.5	23.2
P_2O_5	0.1	0.1	0.4	0.8	1.2	0.3	1.2	0.5	0.8	0.4	1.7	2.4	0.4	0.6	0.3	0.3
SO_2	0.1	0.1	0.2	0.2	0.1	0.2	0.0	0.2	0.1	0.1	0.2	0.2	0.3	0.2	0.4	0.2
ClO	/	/	/	/	/	/	/	/	/	/	/	/	0.1	0.1	0.2	0.4
K_2O	0.8	1.1	1.2	1.9	1.2	1.2	1.3	1.3	1.3	2.0	0.7	1.4	2.0	1.6	1.1	1.4
CaO	1.3	1.5	1.7	2.4	1.5	1.7	1.9	2.2	2.1	2.8	5.0	11.1	0.7	0.6	0.4	0.5
TiO_2	0.1	0.2	0.1	0.1	0.1	0.2	0.3	0.3	0.0	0.3	0.2	0.1	0.4	0.3	0.2	0.3
V_2O_5	0.2	0.0	0.1	0.1	0.0	0.3	0.2	0.1	0.1	0.2	0.3	0.0	0.0	0.2	0.1	0.2
MnO	0.5	1.2	1.1	1.8	1.0	1.1	1.9	1.7	1.4	1.2	0.7	1.1	3.3	1.7	1.6	1.7
FeO	77.2	70.0	66.4	50.4	67.8	63.5	58.1	56.1	57.8	43.7	68.2	40.6	55.5	61.9	72.9	65.2

Metal mass		Dur 3	Dur 3	Dur 3	DUR.40-1	DUR.40-1	DUR.40-1	DUR.40-2	DUR.40-2	DUR.40-2	DUR.40-2	DUR.40-2	DUR.40-2
Inclusion		1	2	3	1	2	3	4	5	6	7	8	9
Trace elements and rare earth in ppm	As	40.3	685.7	2.9	5.2	14.7	8.3	17.1	3.6	nd	1.4	2.9	9.2
	Ba	13067.0	11155.2	13037.9	1763.4	2025.1	2105.9	2425.4	2254.0	2539.4	2345.4	2053.8	2440.8
	Be	161.2	114.2	127.7	275.1	299.1	307.1	377.2	358.3	377.1	359.2	328.8	376.7
	Ce	89.5	74.9	86.3	190.9	211.5	230.4	211.4	241.4	276.0	242.5	219.7	269.1
	Co	49.4	1366.9	2.5	7.6	18.7	6.1	24.7	32.0	22.9	16.0	32.4	74.7
	Cr	nd	nd	nd	448.9	817.8	497.1	609.1	551.8	537.6	340.9	658.4	871.6
	Cs	0.2	nd	4.0	5.1	4.3	6.0	8.8	0.9	1.5	2.2	1.5	2.9
	Cu	40.4	1081.3	4.6	39.6	22.0	27.5	101.8	44.5	14.7	19.7	83.3	133.1
	Eu	7.9	5.6	6.5	18.0	19.1	22.6	20.8	21.3	26.2	23.5	17.6	24.7
	Ga	2033.5	1377.5	2070.6	335.0	382.1	408.7	450.7	414.6	460.4	428.2	369.5	442.9
	Gd	40.2	24.2	33.4	86.2	99.1	114.2	103.2	111.2	130.0	117.3	111.7	133.7
	Ge	11.0	50.0	4.4	19.9	27.0	33.9	24.8	33.6	41.1	35.5	28.5	37.4
	Hf	3.8	2.7	5.5	8.3	10.7	11.2	9.7	10.4	11.9	10.0	10.3	11.2
	La	192.4	126.3	173.0	434.5	455.0	551.8	520.4	569.3	658.0	577.1	512.1	697.1
	Mo	2.8	16.0	0.9	0.3	0.4	0.8	1.4	0.9	4.1	1.5	nd	nd
	Nb	5.6	5.4	8.6	23.0	24.8	24.8	26.2	25.1	29.1	26.5	23.1	30.7
	Nd	127.2	86.3	115.3	275.8	271.3	340.9	299.7	361.3	403.0	360.0	334.2	421.7
	Ni	363.4	5500.9	8.3	7.3	3.7	6.5	24.4	15.9	4.8	11.9	11.7	51.9
	Pb	1.4	21.1	0.4	8.0	11.6	9.7	17.5	7.5	10.1	4.8	8.6	28.5
	Pd	0.1	0.2	nd	1.2	0.7	0.1	nd	nd	0.7	0.7	0.9	0.4
	Pr	27.8	20.2	24.7	55.1	59.8	74.4	64.4	73.7	87.8	77.8	66.5	85.2
	Rb	42.4	64.9	96.5	88.3	96.6	113.8	164.9	117.6	132.0	106.0	108.3	137.2
	Sb	0.8	10.3	nd	nd	0.9	1.1	3.0	nd	nd	nd	0.8	0.3
	Sc	27.3	18.4	23.0	39.8	49.1	46.9	51.5	50.0	46.4	40.4	48.6	56.4
	Sm	26.4	15.0	22.9	63.7	68.8	75.8	71.2	79.9	106.9	86.4	76.3	88.1
	Sn	7.4	16.9	13.7	41.4	52.6	48.7	50.7	38.3	39.5	34.6	35.7	92.8
	Sr	287.4	316.2	320.8	668.7	714.2	808.5	827.1	872.4	963.7	855.6	789.2	918.5
	Ta	0.7	1.0	0.7	1.5	1.7	1.6	1.8	2.0	1.8	1.8	1.9	1.9
	Tb	5.6	3.6	5.1	15.9	17.7	20.1	17.9	21.1	25.9	22.5	18.0	26.3
	Th	11.9	5.2	12.4	26.1	30.8	33.3	34.1	39.0	40.3	35.5	30.0	41.8
	U	169.9	173.1	149.6	46.2	50.0	50.4	57.9	61.8	67.2	64.3	52.6	69.0
	V	27.8	36.1	223.6	137.4	190.5	137.9	173.5	197.4	184.3	146.1	194.0	261.7
	W	0.2	1.9	0.1	5.3	6.6	6.6	4.2	5.8	4.7	4.7	3.1	4.0
	Y	478.9	293.1	414.4	1145.4	1282.2	1463.8	1356.3	1451.0	1658.6	1452.3	1341.9	1792.9
	Yb	22.7	14.5	19.3	69.1	75.0	80.2	79.0	92.5	107.9	86.3	84.1	102.2
	Zn	42.5	658.8	22.0	42.7	59.4	48.4	106.5	45.4	35.5	31.5	71.1	192.2
	Zr	157.5	81.1	207.0	347.0	369.9	385.2	380.8	369.7	428.2	382.8	362.2	612.9

Metal mass		Dur 48-1	Dur 48-1	Dur 48-1	Dur 48-1	Dur 48-1	Dur 48-1	Dur 48-1	Dur 48-1	Dur 48-1	Dur 48-1	Dur 48-2	Dur 48-2	Dur 6	Dur 6	Dur 6	Dur 6
Inclusion		1	2	3	4	5	6	7	8	9	10	1	2	1	2	3	4
Trace elements and rare earth in ppm	As	6.8	26.4	14.2	31.7	12.0	49.9	1192.0	445.1	1401.3	44.2	70.6	31002.9	48.9	8.0	69.3	761.7
	Ba	2368.7	1930.0	2292.1	2325.8	2595.1	3261.8	2726.2	2646.7	3850.5	3254.5	6723.2	2528.9	2266.7	2499.9	2144.3	1034.3
	Be	123.8	112.9	131.0	120.2	123.6	141.1	132.7	146.8	94.6	143.7	195.8	117.4	29.1	43.0	28.4	28.5
	Ce	263.0	238.1	300.0	276.2	250.7	317.2	330.6	303.4	321.5	328.3	378.2	201.6	713.9	638.9	630.8	320.6
	Co	5.2	12.4	10.1	9.3	21.6	92.1	788.6	195.7	540.7	39.6	31.3	8750.0	43.9	1.2	26.7	4012.3
	Cr	nd	nd	nd	nd	nd	nd	nd	nd	nd	nd	nd	nd	38.9	430.2	324.7	2022.0
	Cs	17.5	12.3	13.3	7.7	9.1	15.7	21.5	8.9	14.3	2.3	26.6	nd	20.6	18.3	14.8	17.3
	Cu	37.3	19.2	10.6	8.7	19.8	39.1	119.7	472.2	499.4	448.9	32.5	14938.8	504.8	4.5	321.2	38502.2
	Eu	23.1	22.1	27.8	26.6	23.0	30.6	29.6	25.3	28.1	30.1	43.2	16.9	14.2	15.2	14.3	5.3
	Ga	211.9	219.2	312.9	308.3	375.2	488.9	400.0	425.4	612.8	543.0	834.3	334.7	398.3	459.1	387.0	258.1
	Gd	128.4	102.6	122.2	99.7	107.3	128.4	125.5	101.7	103.5	109.5	177.8	47.0	49.8	59.0	55.1	21.1
	Ge	26.2	24.3	36.2	27.3	31.4	43.6	39.2	46.3	39.5	38.2	37.9	165.8	26.0	26.9	27.7	176.3
	Hf	13.4	11.8	14.1	12.7	13.6	18.2	13.9	13.6	11.1	13.7	6.2	17.5	9.4	14.2	13.9	6.9
	La	270.9	238.0	306.1	272.0	266.2	314.0	328.7	278.7	263.9	296.1	142.9	44.2	284.8	305.5	289.9	99.5
	Mo	0.1	1.4	nd	0.2	0.4	0.5	4.8	2.4	5.1	2.1	0.8	74.5	2.0	1.9	2.7	234.1
	Nb	14.3	12.8	15.6	13.9	15.1	19.2	17.5	14.0	13.7	14.8	7.0	7.3	5.1	30.3	26.8	13.0
	Nd	444.8	382.1	459.9	412.5	388.4	473.5	487.9	410.0	439.5	465.9	607.8	113.5	358.2	401.7	368.0	109.0
	Ni	3.6	10.6	1.5	18.9	14.6	195.2	1011.2	622.3	2409.7	55.4	7.1	17404.6	118.3	1.7	89.4	3787.4
	Pb	0.5	0.8	2.0	2.5	8.8	5.9	1.1	8.8	5.8	4.5	6.5	133.4	19.4	1.5	5.8	718.0
	Pd	0.7	0.2	0.4	0.5	0.6	0.9	0.7	0.2	0.2	0.7	0.3	nd	0.3	0.5	0.6	1.1
	Pr	78.1	67.9	84.5	76.4	71.6	87.5	91.6	77.3	79.1	84.4	76.8	14.4	85.3	87.5	83.7	26.8
	Rb	152.3	90.0	125.6	100.2	100.1	136.9	145.3	116.0	134.7	121.2	138.9	25.4	311.0	233.5	197.5	113.6
	Sb	nd	nd	0.3	0.5	nd	nd	5.0	3.1	7.3	1.2	nd	53.8	0.7	0.2	0.9	93.3
	Sc	97.5	53.2	77.9	56.8	57.2	41.1	16.0	nd	nd	nd	nd	660.1	73.7	90.6	77.4	62.7
	Sm	104.6	92.6	112.5	97.0	89.3	118.1	119.5	104.9	108.7	122.3	171.5	38.5	65.2	71.4	69.5	29.1
	Sn	11.5	11.8	14.3	7.5	21.9	29.7	20.0	17.6	19.7	25.8	47.4	156.7	13.8	13.5	16.5	178.3
	Sr	123.6	99.2	108.5	116.1	141.6	166.2	126.7	142.2	167.2	161.8	199.9	443.5	188.7	184.1	163.9	719.9
	Ta	0.5	0.6	1.0	0.7	0.2	0.7	0.8	1.5	0.8	1.2	nd	19.5	1.3	1.7	1.9	66.5
	Tb	15.2	13.0	16.7	14.0	14.4	17.4	17.3	15.1	15.8	18.2	23.0	5.8	7.3	8.8	8.0	2.9
	Th	21.5	17.9	24.3	21.4	22.1	27.9	25.4	21.7	20.3	23.0	14.0	4.3	32.0	36.6	39.3	12.8
	U	14.4	12.1	14.9	14.0	13.0	14.5	16.0	14.0	16.7	15.6	25.6	19.3	39.5	31.3	34.9	15.1
	V	1077.5	706.8	740.7	771.5	643.0	1521.9	887.7	789.2	727.7	718.9	525.0	316.9	29.5	707.7	553.2	524.3
	W	nd	nd	1.0	nd	4.0	10.1	0.8	5.4	3.1	3.6	nd	149.6	0.6	0.1	0.9	151.0
	Y	863.9	747.5	942.6	807.9	892.9	1048.5	1005.6	876.4	835.0	960.2	1039.2	185.3	238.5	293.9	264.7	109.2
	Yb	63.6	55.0	64.2	55.3	57.0	74.9	70.3	55.3	54.4	57.6	69.7	9.6	23.0	27.4	25.4	10.1
	Zn	nd	11.7	23.8	6.7	43.9	59.8	21.4	379.4	292.1	90.6	nd	7076.6	181.1	10.1	105.1	14393.1
	Zr	507.5	448.5	569.4	469.3	540.3	678.7	625.3	740.4	461.4	576.6	356.1	3056.7	429.7	602.7	548.6	562.7

Supplementary material Table S4